Numerical accuracy of the linear muffin-tin orbitals method for dilute metallic alloys

1992 J. Phys.: Condens. Matter 4 3759

(http://iopscience.iop.org/0953-8984/4/14/008)

J. Phys.: Condens. Matter 4 (1992) 3759–3772. Printed in the UK

Numerical accuracy of the linear muffin-tin orbitals method for dilute metallic alloys

C Koenig and P Jund
Université Louis Pasteur, IPCMS, 4 rue Blaise Pascal, 67070 Strasbourg, France

Received 9 October 1991, in final form 11 December 1991

Abstract. Some analytical aspects of the linear muffin-tin orbitals (LMTO) method for metals and alloys are considered here, which are directly related to the accuracy of the numerical program giving the self-consistent electronic structure of dilute impurities. It is first shown that the existence of mathematical singularities at special energies within the valence energy range in the LMTO formalism induces no discontinuity in physical quantities such as the local density of states or the total displaced charge versus energy. Then, the numerical effects of the use of more than one energy panel for the valence states in the pure matrix and in the dilute alloy are compared, and we discuss the existence of a limit to the intrinsic accuracy of an impurity program for a given matrix of type X, by considering a fictitious alloy $\underline{X}X$. Finally we give, as an example, our results for dilute Al alloys, which, in contrast to a recent publication, are very close to those obtained by the Green function method.

1. Introduction

Ab initio self-consistent calculations of the electronic structure of metals and alloys provide a realistic description of the charge and magnetic moment distributions, without any adjustable parameters. This type of calculation has been developed over the last decade within the Green function theory initiated by Korringa, Kohn and Rostoker (KKR) (see e.g. [1, 2]), and the perturbation on the neighbours of the impurity is now currently included in the self-consistent process [3]. We have shown [4–6] that comparable results can be obtained within the linear muffin-tin orbitals (LMTO) method, which avoids the tedious calculations inherent in the KKR method.

The fundamental approximation leading from the KKR to the LMTO formalism is the neglect of the kinetic energy $\mathcal{K}^2 = E - V_{\mathrm{MTZ}}$ of the electrons outside the atomic spheres. The successive steps of this theory have been extensively developed in the literature [5, 7]. For ordered compounds, energy-independent Bloch functions are then constructed from 'muffin-tin' orbitals of logarithmic derivative $D = -l - 1$ at the atomic radius S, centred on each atom of the different sublattices; for dilute alloys, the LMTO formalism is directly obtained from the multiple scattering theory by setting $\mathcal{K}$ equal to zero. In both cases, metals or alloys, approximate wavefunctions of logarithmic derivative D are constructed by linear combination of exact solutions $\varphi_{l\nu}(r)$ of Schrödinger's equation and their energy derivatives $\dot{\varphi}_{l\nu}(r)$, with the help of a Laurent series expansion of $1/(D - D_{l\nu})$. The aim of the present work is to discuss the numerical implications of these different approximations and to analyse their consequences on the intrinsic

0953-8984/92/143759 + 14 $04.50

accuracy of the electronic structure programs for pure metals as well as for dilute impurities. In order to simplify the notation as much as possible, we limit the discussion to the case of an isolated impurity in a monatomic metal within the single-site approximation, the extension of the conclusions to less localized defects being straightforward.

This paper is organized as follows. In section 2, the scattering of electrons by an isolated atom of Wigner–Seitz radius S is considered in the limit $\mathcal{K} \to 0$ outside the atomic sphere. For each value of the orbital momentum l, three energies E_l^0, E_l^* and $E_l^\dagger$ are defined, which will play a special part in the following.

In section 3 the LMTO method for pure metals is considered, and two points are discussed: (1) the numerical accuracy of the linearization of the 'muffin-tin' orbitals, especially above E_l^0, related to the number of energy panels used to describe the conduction states; (2) the necessity of using the tetrahedron method for the computation of the number of occupied states for each symmetry (this point is important for the impurity case).

Section 4 is devoted to the LMTO theory for dilute alloys. It is shown that, although the limit $\mathcal{K} \to 0$ introduces analytical discontinuities at the special energies in the LMTO expressions of some functions that are continuous in the KKR theory (such as the scattering t-matrix), this induces no discontinuity in the physical quantities such as the total displaced charge or the partial densities of states.

Finally, we discuss in section 5 the intrinsic accuracy of the different steps of the LMTO program for dilute impurities. The additional numerical difficulty presented by the computation of the total number of occupied states for each symmetry in a non-periodic alloy is especially stressed by considering fictitious impurities X diluted in a metal of the same chemical species: $\underline{\mathrm{X}}\mathrm{X}$. A few examples of magnetic or non-magnetic impurities in aluminium are given in order to show that, contrary to a recently published work [8], our results are always close to those of the KKR theory.

2. Special energies E_l^0, E_l^* and $E_l^\dagger$

The fundamental parameter of these methods is the logarithmic derivative of the radial wavefunction $\varphi_l(E, r)$ at the surface of the atomic sphere ($r = S$):

$$D_l(E) = S[\varphi_l'(E, r)/\varphi_l(E, r)]_{r=S}. \tag{1}$$

It is a monotonically decreasing function of the energy between successive vertical asymptotes at energies E_{li}^0 such that $\varphi_l(E_{li}^0, S) = 0$. The index i of successive branches of $D_l(E)$ indicates the number of nodes of the wavefunction between 0 and S, in a similar fashion as the principal quantum number n of an isolated atom. In the energy range of the valence states, one or two branches $D_{li}(E)$ can play a part, depending on whether the Fermi level E_F lies below or above the nearest E_{li}^0. In the following, we shall omit whenever possible the branch index i of the valence states.

In the KKR formalism an isolated spherical atomic potential is described by a scattering t-matrix element:

$$t_l(\mathcal{K}) = -(1/\mathcal{K})\, \mathrm{e}^{\mathrm{i}\eta_l(\mathcal{K})} \sin[\eta_l(\mathcal{K})] \tag{2}$$

where $\eta_l(\mathcal{K})$ is the phase shift of the waves for symmetry l. It is well known that its value

at zero kinetic energy is proportional to the number N_{Cl} of bound states of l symmetry (per spin) in the atomic potential:

$$(1/\pi)(2l+1)\eta_l(0) = N_{Cl}. \tag{3}$$

The LMTO limit has to be performed without modifying the energy inside the atomic sphere. It is obtained by an artificial increase of the potential outside the sphere, from its constant value V_{MTZ} up to the energy E. Therefore, in this limit, one has to consider an energy-dependent LMTO potential for each isolated atom: this potential is identical to the atomic potential in the atomic sphere, but is different for each energy outside this sphere. The main consequence of this is that, for E greater than an energy E_l^* such that $D_l(E_l^*) = -l-1$ in the valence branch, the corresponding LMTO potential allows a supplementary *bound* state at E_l^*, of wavefunction $\varphi_l(E_l^*, r)$ for $r < S$, with a tail proportional to r^{-l-1} outside the sphere. Following the notation of [7], let us call $\chi_L(r)$ this orbital, centred on the atom and defined in the whole space. Then, equation (3), which is valid for an atomic potential, has to be replaced by

$$(1/\pi)(2l+1)\eta_l(0) = N_{Cl} + (2l+1)\Theta(E - E_l^*) \tag{4}$$

where Θ is the Heaviside function.

Up to now, we have defined the special energies E_l^0 and E_l^*. The last special energy is obtained by considering the LMTO limit of $t_l^{-1}(\mathcal{K})$ [4]:

$$P_l(E) = 2(2l+1)[D_l(E) + l + 1]/[D_l(E) - l]. \tag{5}$$

This function is singular at an energy $E_l^\dagger$ such that $D_l(E_l^\dagger) = l$. This singularity corresponds in the KKR formalism to a zero scattering matrix element, hence to a phase shift multiple of π. The cross section is then also zero, which corresponds to a transparency of the potential for that energy and symmetry.

It must be noted that the special part played in the LMTO theory by E_l^* and $E_l^\dagger$ is a mathematical artefact of the limit $\mathcal{K} \to 0$ in the KKR formalism. No singularity of the physical quantities is expected at these energies.

3. Periodic matrix

For periodic compounds, the Bloch functions $\chi_L^k(r)$, where $L = (l, m)$, are built from linear combinations of 'muffin-tin' orbitals of logarithmic derivatives $-l-1$ at S, which are the orbitals χ_L of energy $\bar{E}_l^*$ described in section 2:

$$\chi_L^k(r) = \sum_{R^n} e^{ik\cdot R^n} \chi_L(r - R^n).$$

This leads to a very simple formulation of the matrix elements of the Hamiltonian, and the total wavefunction in the crystal for each band j:

$$\psi_j^k(r) = \sum_L A_{Lj}^k \chi_L^k(r)$$

is given by a simple diagonalization

$$\sum_L A_{Lj}^k (\langle \chi_{L'}^k | H | \chi_L^k \rangle - E_j^k \langle \chi_{L'}^k | \chi_L^k \rangle) = 0. \tag{6}$$

For $r < S$, the 'muffin-tin' orbitals $\bar{\phi}_l(\bar{E}_l^*, r)$ of logarithmic derivative $-l-1$ are

Table 1. Special energies for pure Cu (Ryd). $E_F = -0.1143$ Ryd, $E_B = -0.8211$ Ryd (bottom of the band). The energies marked > or < are well outside the valence panel.

	E_l^0	E_l^*	$E_l^\dagger$
4s	>	−0.428	−0.821
4p	>	0.541	−0.843
3d	−0.228	−0.312	<
4d	>	>	0.180

obtained, like any orbital of energy E and logarithmic derivative $\bar{D}$, from the normalized numerical solution $\bar{\varphi}_{lv}(r)$ of the Schrödinger equation at an arbitrarily fixed energy $\bar{E}_{lv}$ by the linear combination:

$$\bar{\phi}_l(E(\bar{D}_l), r) = \bar{\varphi}_{lv}(r) + \bar{\omega}_l(\bar{D}_l)\dot{\bar{\varphi}}_{lv}(r) \tag{7}$$

which has to be normalized when necessary. $\bar{D}_l$ is deduced from the Laurent series:

$$\frac{1}{\bar{D}_l(E) - \bar{D}_{lv}} = -\frac{S\bar{\varphi}_{lv}^2(S)}{E - \bar{E}_{lv}} - S\bar{\varphi}_{lv}(S)\dot{\bar{\varphi}}_{lv}(S) + (E - E_{lv})S\bar{\varphi}_{lv}^2(S)\langle\dot{\bar{\varphi}}_{lv}^2(r)\rangle + o(E - \bar{E}_{lv}). \tag{8}$$

The validity of expression (7) has been extensively discussed by Andersen [7]. It is correct to third order in energy provided that $\bar{E}_{lv}$ is chosen in a region of negative logarithmic derivative $\bar{D}_l$, i.e. in the vicinity of $\bar{E}_l^*$. But its use in intermediate zones between two branches i and $i+1$ just above $\bar{E}_{il}^0$, characterized by a high positive value of $\bar{D}_l$, may induce non-negligible numerical errors. In these regions a Taylor series truncated to third order

$$\bar{\phi}_l(E, r) = \bar{\varphi}_{lv}(r) + (E - \bar{E}_{lv})\dot{\bar{\varphi}}_{lv}(r) + \tfrac{1}{2}(E - \bar{E}_{lv})^2\ddot{\bar{\varphi}}_{lv}(r) + \tfrac{1}{6}(E - \bar{E}_{lv})^3\dddot{\bar{\varphi}}_{lv}(r) \tag{9}$$

which is normalized, is safer. Such an intermediate zone occurs for example in Cu just above the 3d 'band', between $\bar{E}_{3d}^0$ and E_F (table 1 and figure 1), so that this metal will be a good test for the accuracy of the programs.

In a one-panel calculation, where each symmetry l is described with one $\bar{E}_{lv}$ chosen in the range of negative $\bar{D}_l$, the eigenenergies E_j^k obtained from (6) have a large spectrum, which often contains intermediate zones for some symmetries. However, the weights $|C_{Lj}^k|^2$ of these symmetries, which can be deduced from the eigenvectors A_{Lj}^k, are in fact very small in these zones, the main part of the band of l symmetry being located in the region of negative D_l, i.e. in the vicinity of $\bar{E}_l^*$. Therefore, the partial densities of state per atom:

$$\bar{n}_L(E) = \sum_{jk} |C_{Lj}^k|^2\, \delta(E - E_j^k)$$

are generally very good in the energy regions where they are high, and very small in the regions where the method itself is not very accurate. A calculation with three panels for Cu, replacing (7) by a Taylor series (9) for the 4d states in the upper panel ($E > \bar{E}_{3d}^0$), gives a nearly identical result as the one-panel calculation (figure 1). For most of the ordered compounds, except for those presenting semi-core states [9], the use of more than one panel for the occupied valence states is generally not justified.

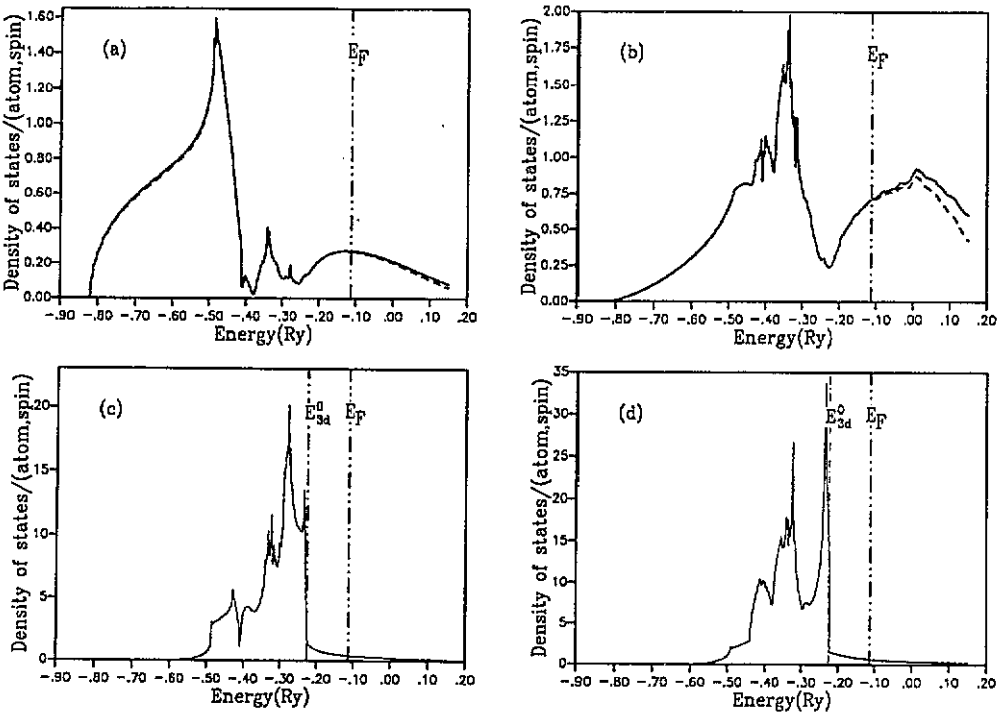

Figure 1. Densities of states for s (*a*), p (*b*), d_{12} (*c*) and d_{25} (*d*) symmetries for pure Cu: (– – – –) one-panel calculations; (———) three panels.

In the calculation of the radial density of valence electrons:

$$\bar{\rho}_L(r) = \int_{E_B}^{E_F} |\bar{\phi}_l(E, r)|^2 \bar{n}_L(E)\, dE \tag{10}$$

in which an integral has to be performed from the bottom E_B of the valence states to the Fermi level, the Taylor series (9) for $\bar{\phi}_l(E, r)$ is preferable to the LMTO expression (7), since it is also valid above $\bar{E}^0_l$. Then (10) can be separated into different terms depending upon the successive moments of $\bar{n}_L(E)$. The important point for the rest of this paper is that the first of these moments, i.e. the number of occupied states up to the energy E on the considered site (located at the origin 0):

$$\bar{N}^0_L(E) = \int_{E_B}^{E} \bar{n}_L(E')\, dE' \tag{11}$$

is calculated, together with $\bar{n}_L(E)$, by a tetrahedron method [10]; $\bar{N}^0_L(E)$ is simply proportional to the occupied volume below E in the Brillouin zone, so that the integral (11) has never to be performed numerically.

This numerical integration has to be avoided, owing to the rough behaviour of $\bar{n}_L(E)$. Table 2 shows the value of $\bar{N}^0(E_F)$ calculated by (11) for Cu, versus the number of k-points in the irreducible wedge of the Brillouin zone and the energy scale, with a Fermi level fixed by the condition that $\bar{N}^0(E_F)$ calculated by the tetrahedron method is equal to (11). If (11) is substituted for the tetrahedron calculation in the self-consistent

Table 2. Number of occupied states for Cu given by integral (11) versus the number of k-points and the energy scale.

Number of k-points	961	1638	2030	961	2030
ΔE (Ryd)	0.001	0.001	0.001	0.0005	0.0005
$\bar{N}^{\mathrm{tl}}(E_{\mathrm{F}})$	10.997	11.0006	10.994	11.003	11.002

Table 3. Test on Cu: number of electrons per atom, symmetry and spin for the pure matrix with one (1) or five (5) panels for the radial charge, and for a Cu impurity treated with five panels.

Number of electrons	s/spin	p/spin	d/spin	N^0_{tot}
Cu(1)	0.3481	0.3719	4.7800	11.0000
Cu(5)	0.3479	0.3718	4.7803	11.0000
Cu(1)Cu(5)	0.3482	0.3721	4.7809	11.0025
Cu(5)Cu(5)	0.3476	0.3711	4.7781	10.9938

Table 4. Same as table 3, but for Fe.

Number of electrons	Spin	s/spin	p/spin	d/spin	N^0_{tot}	M^0_{tot}
Fe(1)	↓	0.3277	0.4268	2.1428	8.0000	2.2053
	↑	0.3158	0.3737	4.4131		
Fe(5)	↓	0.3277	0.4265	2.1433	8.0000	2.2050
	↑	0.3158	0.3735	4.4132		
Fe(1)Fe(5)	↓	0.3292	0.4307	2.1812	8.0275	2.1450
	↑	0.3170	0.3764	4.3928		
Fe(5)Fe(5)	↓	0.3271	0.4253	2.1246	7.9923	2.2382
	↑	0.3154	0.3727	4.4271		

procedure, one obtains generally weak variations from one iteration to the next in the numerical integration of the high peaks of the densities of states, leading to small variations of $\bar{N}_L(E)$ and hence to a small deterioration of the quality of the convergence.

Finally, a question can be raised on the validity of a Taylor development of $\bar{\phi}_l(E, r)$ around one single $\bar{E}_{l\nu}$ in (10), since the wavefunction is not small far from $\bar{E}_{l\nu}$. Therefore, two self-consistent calculations for pure Cu and pure magnetic Fe have been performed: in both calculations one panel is used to compute $\bar{n}_L(E)$; then (10) is calculated with one panel for the first calculation and with five panels in the second one. The self-consistent numbers of electrons are given in tables 3 and 4; the discrepancies between the two calculations are less than 0.001 electron.

4. Dilute alloys

The electronic density on the impurity site and the total number of displaced states in the alloy are given by the Green function G of the alloy, which is related to the Green function $\bar{G}$ of the pure matrix by a Dyson equation. The simplest formulation of this equation is the one given by Harris [11]. Let $\mathcal{R}_l^n(r)$ be the real wavefunction of energy E on the site n, proportional to $\mathcal{H}\{j_l(\mathcal{H}r)\cot[\eta_l(\mathcal{H})] - n_l(\mathcal{H}r)\}$ for $r \gg S$, and G^S the Green function for an isolated atom; then

$$G(\boldsymbol{r}+\boldsymbol{R}^n, \boldsymbol{r}'+\boldsymbol{R}^{n'}) = \sum_L Y_L(\hat{r})G_L^{Sn}(r,r')Y_L^*(\hat{r}')\delta_{nn'}$$

$$+ \sum_{LL'} Y_L(\hat{r})\mathcal{R}_l^n(r)(G_{LL'}^{nn'} - t_l^n\delta_{LL'}\delta_{nn'})\mathcal{R}_{l'}^{n'}(r')Y_{L'}^*(\hat{r}') \tag{12}$$

where the imaginary part of G^S cancels the one of t_l^n in the multiple scattering term [11]. The structural Green function $G_{LL'}^{nn'}(E)$ is then given by

$$G_{LL'}^{nn'} = \bar{G}_{LL'}^{nn'} + \sum_{L'',n''} \bar{G}_{LL''}^{nn''}[(\bar{t}_{l''}^{n''})^{-1} - (t_{l''}^{n''})^{-1}]G_{L''L'}^{n''n'}. \tag{13}$$

In the single perturbed site approximation, the total number of displaced electrons up to E in the whole crystal is

$$N_L^{\mathrm{tot}}(E) - \bar{N}_L^{\mathrm{tot}}(E) = -(1/\pi)\,\mathrm{Im}\ln[1 + \bar{G}_{LL}^{00}(1/t_l - 1/\bar{t}_l)] \tag{14}$$

where we have dropped the site index $n = 0$ for t and $\bar{t}$. By noting that $\eta_l(\mathcal{H}) = \arg t_l = \mathrm{Im}\ln t_l$, (14) can also be written as

$$N_L^{\mathrm{tot}}(E) - \bar{N}_L^{\mathrm{tot}}(E) = (1/\pi)\{\eta_l(\mathcal{H}) - \bar{\eta}_l(\mathcal{H}) - \mathrm{Im}\ln[(t_l/\bar{t}_l)(1 + \bar{G}_{LL}^{00}(1/t_l - 1/\bar{t}_l))]\}. \tag{15}$$

This last expression is directly obtained in the formulation of Podloucky *et al* [12], which we have used earlier [5].

We have already detailed in [5] how to get in a systematic way the LMTO expressions of these quantities. The LMTO limit of $\mathcal{R}_l^n(r)$ is $\sqrt{(\dot{P}_l^n)}\phi_l^n(E,r)$, where $\phi_l^n(E,r)$ is the normalized wavefunction of energy E in the nth sphere of the alloy, and

$$\dot{P}_l^n(E) = \partial P_l^n(E)/\partial E = 2(2l+1)^2[-\dot{D}_l^n(E)]/[D_l^n(E) - l]^2. \tag{16}$$

The LMTO limit of $G_{LL'}^{nn'}$ is the Green function $\Gamma_{LL'}^{nn'}$, which is related to the function $J_{LL'}^{nn'}$ defined in [5] by

$$\Gamma_{LL'}^{nn'} = J_{LL'}^{nn'} + (1/P_l^n)\delta_{LL'}\delta_{nn'}$$

and satisfies a simpler Dyson equation

$$\Gamma_{LL'}^{nn'} = \bar{\Gamma}_{LL'}^{nn'} + \sum_{L''n''} \bar{\Gamma}_{LL''}^{nn''}(\bar{P}_{l''}^{n''} - P_{l''}^{n''})\Gamma_{L''L'}^{n''n'}. \tag{17}$$

The numerical calculation of $\bar{\Gamma}_{LL''}^{nn''}$ (or $\bar{J}_{LL'}^{nn'}$) has been detailed in [5]. For cubic symmetries

and $l \leqslant 2$, the intra-site elements are diagonal when expressed in cubic harmonics, and are given by

$$\bar{\Gamma}^{00}_{LL} = (1/\dot{\bar{P}}_l)[\bar{f}_L(E) + \dot{\bar{P}}_l/\bar{P}_l - 1/(E - \bar{E}^*_l)] - i\pi\,\bar{n}_L(E)/\dot{\bar{P}}(E) \tag{18}$$

where $\bar{f}_L(E)$ is the Hilbert transform of $\bar{n}_L(E)$. In the single-site approximation, the total number of displaced electrons in the crystal for the symmetry L is then (per spin)

$$N^{\text{tot}}_L(E) - \bar{N}^{\text{tot}}_L(E) = -(1/\pi)\,\text{Im ln}[1 + \bar{\Gamma}^{00}_{LL}(P_l - \bar{P}_l)] \tag{19}$$

$$= (1/\pi)\{\eta_l(0) - \bar{\eta}_l(0) - \text{Im ln}[(\bar{P}_l/P_l)(1 + \bar{\Gamma}^{00}_{LL}(P_l - \bar{P}_l))]\} \tag{20}$$

which are the LMTO limits of (14) and (15), and where again the site index $n = 0$ has been dropped for P_l and $\bar{P}_l$.

If the contribution $(N_{CL} - \bar{N}_{CL})$ of the core states of the impurity and the matrix is isolated and the phase shifts set to zero at the bottom of the valence band:

$$(1/\pi)[\eta_l(0) - \bar{\eta}_l(0)] = \Theta(E - E^*_l) - \Theta(E - \bar{E}^*_l) \tag{21}$$

then (19) and (20) give the contribution of the valence states to the total displaced charge, *including* the one of the artificial bound states at energies E^*_l and $\bar{E}^*_l$ in the isolated LMTO potentials, and generalized phase shifts $\Lambda_L(E)$ for the valence states can be defined by

$$N^{\text{tot}}_L(E) - \bar{N}^{\text{tot}}_L(E) = (1/\pi)\Lambda_L(E). \tag{22}$$

The total displaced charge is a continuous variable of E in the KKR formalism. Its LMTO expression must also be continuous, despite the singularities of P_l at $D_l = l$ and P_l^{-1} at $D_l = -l - 1$.

It is easy to verify that (19) has no singularity at E^*_l or $\bar{E}^*_l$. In (20) the same compensation occurs as in (15): in the vicinity of E^*_l, $P_l(E)$ can be written as

$$P_l(E) \simeq \dot{P}_l(E^*_l)(E + i\varepsilon - E^*_l)$$

ε being a small positive imaginary part. When E becomes greater than E^*_l, the argument of $P_l(E)$ is reduced by π whereas a new artificial bound state appears in the LMTO potential. Hence, at $E = E^*_l$, the discontinuity of Im ln P_l cancels exactly the one of $\eta_l(0)$ given by (21). The same cancellation occurs at $\bar{E}^*_l$.

In the vicinity of $\bar{D}_l = l$, the divergence of $\bar{P}_l$ is compensated by a zero of $\bar{\Gamma}$ in (19) and (20). For $D_l = l$, (20) has no singularity but (19) diverges as well as (13), which is in fact only valid for $t_l(E) \neq 0$. As was said before, $E^\dagger_l$ is an energy for which the defect is transparent and the scattering formalism has to be reconsidered from the beginning. The generalized phase shift $\Lambda_L(E)$ defined in (22) can also be obtained by

$$\Lambda_L(E) = -\text{Atan}\{(P_l - \bar{P}_l)\,\text{Im}\,\bar{\Gamma}^{00}_{LL}/[1 + (P_l - \bar{P}_l)\,\text{Re}\,\bar{\Gamma}^{00}_{LL}]\} \tag{23}$$

which does not display any singularity at $E^\dagger_l$ or $\bar{E}^\dagger_l$. This phase shift is a continuous function of E in the whole range of energies, so that any numerical discontinuity of (23) has to be corrected.

It is finally easy to verify that the local density on the impurity

$$n_L(E) = -(1/\pi)\dot{P}_l(E)\,\text{Im}\,\Gamma^{00}_{LL}(E) = (\dot{P}_l/\dot{\bar{P}}_l)\bar{n}_L(E)/\{[1 + (P_l - \bar{P}_l)\,\text{Re}\,\bar{\Gamma}^{00}_{LL}]^2 + [(P_l - \bar{P}_l)\,\text{Im}\,\bar{\Gamma}^{00}_{LL}]^2\} = \alpha_L(E)\bar{n}_L(E) \tag{24}$$

has no singularity at the special energies.

5. Numerical aspects and examples

The radial density of electrons on the impurity site is obtained from

$$\rho_L(r) = \int_{E_B}^{E_F} |\phi_l(E, r)|^2 n_L(E)\, dE \tag{25}$$

and then the atomic potential is recalculated in the same way as for the matrix, allowing a new iteration to start. However, the calculation for impurities presents two numerical difficulties compared to a band-structure calculation of a pure matrix.

5.1. Accuracy of the calculation of $P_l(E)$ and $\dot{P}_l(E)$

The density of states on the impurity (24) depends upon these two functions for the matrix and impurity potentials in the whole range of the valence band. These quantities are large in the intermediate regions between two branches of $D_l(E)$, where the Laurent series (8) for $\bar{D}_l(E)$, or its equivalent for $D_l(E)$, is not precise. Therefore, the calculation of (5) and (15) from (8) may not be very accurate in these intermediate regions. It is then preferable to use a Taylor series to third order of type (9) for $\phi_l(E)$ and for $\phi_l'(E)$ in the two expressions:

$$P_l(E) = 2(2l+1)[S\phi_l'(E,S) + (l+1)\phi_l(E,S)]/[S\phi_l'(E,S) - l\phi_l(E,S)] \tag{26}$$

$$\dot{P}_l(E) = 2[(2l+1)^2/S]/[S\phi_l'(E,S) - l\phi_l(E,S)]^2. \tag{27}$$

For the matrix, an additional local expansion around $\bar{E}_l^*$ has to be considered in the vicinity of this energy in order to get correct numerical compensation of the two last terms in the brackets in equation (18).

Figure 2 compares to their exact values the two functions $P_l(E)$ and $\dot{P}_l(E)$ for Cu, calculated by both methods with one or five energy panels. The necessity for several panels is now evident: as the regions of high $n_L(E)$ may be very different from those of high $\bar{n}_L(E)$ (for example in the case of a resonance), precise values of $P_l(E)$ and $\dot{P}_l(E)$ are needed in (24) for the matrix and the impurity in the whole range of the valence states. The LMTO calculation of $P_l(E)$ is slightly better than the third-order calculation in the regions where D_l is negative, as expected. But the values of $\dot{P}_l(E)$ calculated by (27) are everywhere better than what is obtained from (8) and (16), and particularly in the intermediate zone above E_{3d}^0.

5.2. Accuracy of the calculation of $n_L(E)$ and $\rho_L(r)$: test on CuCu and FeFe

A very precise test of the numerical accuracy of the program is to perform a self-consistent calculation of the electronic structure of an 'impurity' of type X in a matrix of the same type. Our previous tests on Al, FeAl and ferromagnetic Fe [5] display small numerical differences between the 'impurity' and the equivalent atom in the matrix, which we attributed to the lack of 'combined corrections' beyond the atomic sphere approximation in the impurity cell. This argument, which has recently been put forward again by Singh [8], is in fact not correct. The effect of the combined corrections is contained in the numerical values of $\bar{n}_L(E)$ and is transmitted to the impurity via equation (24). By considering (24), (10) and (25), it can be seen that, if the initial potential on the impurity is *identical* to the matrix potential, the densities of states and the charge distributions should also be identical. Then the self-consistency on the impurity should

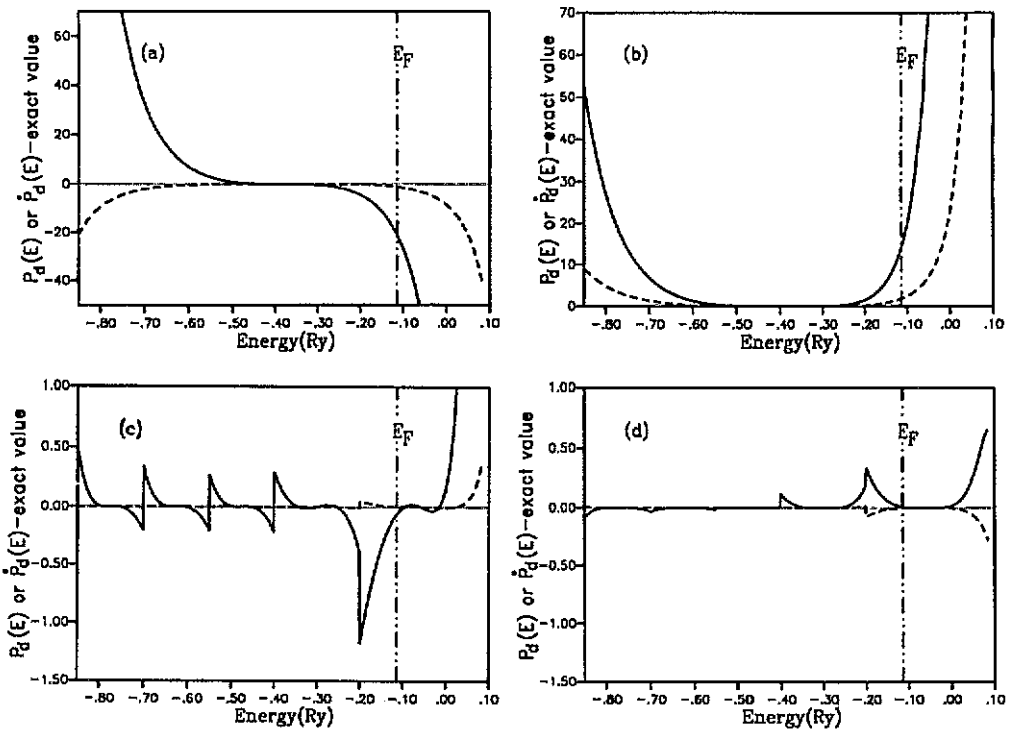

Figure 2. Difference between the calculated functions $P_d(E)$ (– – – –) and $\dot{P}_d(E)$ (——) for pure Cu and their exact numerical values. (*a*) One panel and LMTO formulae (5), (8) and (16). (*b*) One panel and third-order Taylor series in (26) and (27). (*c*) Same as (*a*) with five panels. (*d*) Same as (*b*) with five panels.

lead to no difference in the results, provided that the matrix calculation is well converged. The small numerical differences observed on the fictitious 'impurities' are in fact only due to a slight numerical inaccuracy of the impurity program, which is almost impossible to avoid. We want here to emphasize this point with the examples of CuCu and FeFe.

In (25) the wavefunction is calculated by a Taylor series to third order. The successive moments of the density of states $n_L(E)$ are calculated in each panel from the local number of electrons on the impurity site:

$$N_L^0(E) = \int_{E_B}^{E} n_L(E')\,\mathrm{d}E' \tag{28}$$

which is the equivalent of (11). However, the alloy is not a periodic system, so that the only way to compute $N_L^0(E)$ is to perform the integration (28) numerically. It is then evident that even at the first iteration it will be different from $\bar{N}_L^0(E)$ so that the charge density $\rho_L(r)$ will also be slightly different from $\bar{\rho}_L(E)$, even if the same panels are used for its calculation in the matrix and on the impurity. In tables 3 and 4, the only source of numerical discrepancies between Cu(5) and Cu(5) or Fe(5) and Fe(5) at the first iteration is the numerical integration of the impurity density of states. This induces a slight difference between $P_l(E)$ and $\bar{P}_l(E)$ in the next iteration, and both effects are cumulated during the self-consistent process.

Table 5. Impurities in Al. N^0 = total number of valence electrons in the impurity cell; M^0 = local magnetic moment; $N_{tot} = \bar{Z} - \bar{N}_C + (1/\pi)\,\Sigma_{L\sigma}\,\Delta^{\sigma}_{L}(E_F)$; X = impurity of type X without screening rule (29); X(+) = with screening rule (29); X* = non-magnetic X impurity. (*a*) Our results (LMTO); (*b*) Deutz *et al* [2] (KKR); (*c*) Singh [8] (LMTO).

(*a*)	N^0	N_{tot}	M^0
Al(+)	3.000003	3	0
Cu	11.236	11.065	0
Cu(+)	11.156	11	0
Fe	8.203	8.400	1.828
Fe(+)	7.858	8	2.464
Mn*	7.181	7.548	0
Mn*(+)	6.705	7	0
Mn	7.135	7.434	2.615
Mn(+)	6.792	7	3.190
(*b*)	N^0	N_{tot}	M^0
Cu	11.26	11.00	0
Fe*	8.31	8.39	0
Fe	8.31	8.39	1.78
Mn*	7.27	7.52	0
Mn	7.27	7.51	2.53
Mn(+)	—	7	3.18
(*c*)	N^0	N_{tot}	M^0
Al	3.005	—	0
Cu	11.273	11.078	0
Cu(+)	11.103	10.888	0
Fe*	8.279	8.402	0
Fe*(+)	7.895	8.000	0
Mn*	7.232	−2.492	0
Mn*(+)	7.899	2.062	0

In order to put the two calculations on the same footing, one could also calculate (11) numerically for the matrix, but this induces a loss of precision in the convergence for the pure matrix and hence does not improve the final result on the 'impurity'. A more elegant way to circumvent this difficulty is to make use of the complex-energy technique [13]: far from the real axis the Green function is smooth and its numerical integration easy. This technique has been used in [5] for the impurity but not for the matrix.

Tables 3, 4 and 5 give an estimate of the intrinsic accuracy of the impurity program, which varies from one case to the other. The difference in the number of conduction electrons in the 'impurity' cell and in the matrix is of about 0.000 003 electron for Al, which is a very easy case. The precision is of about 0.005 electron for Cu, and drops down to 0.02 electron and 0.04 μ_B for Fe. All the results presented below have been obtained from a one-panel calculation for the pure matrix and a five-panel calculation

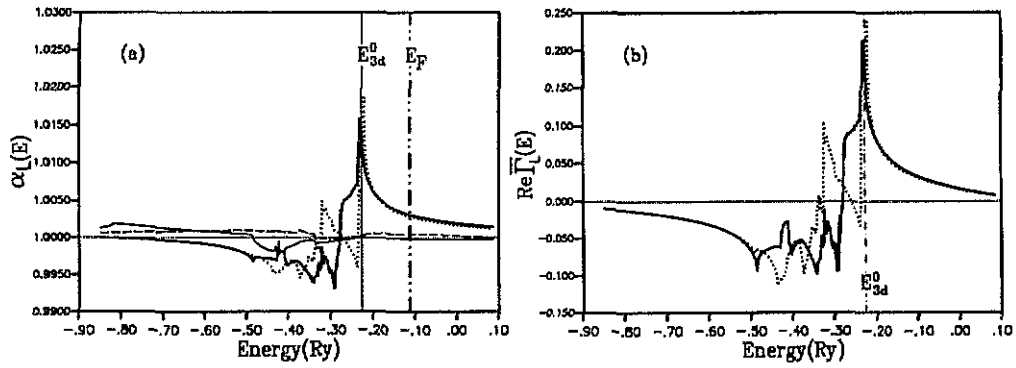

Figure 3. (*a*) Coefficient $\alpha_L(E)$ for the four cubic symmetries in pure Cu: (– – –) s states; (———) p states; (———) d_{12} states (. . . .) $d_{25'}$ states. (*b*) Real part of $\bar{\Gamma}^{00}_{LL}(E)$ for d_{12} (———) and $d_{25'}$ (. . . .). Its imaginary part is approximately proportional to the opposite of $\bar{n}_L(E)$ given in figures 1(*c*) and (*d*).

for $\bar{P}_L(E)$, $\dot{\bar{P}}_L(E)$ and all the impurity program, with a Taylor series to third order for the wavefunctions in (10), (25), (26) and (27).

Figure 3 displays the self-consistent values of the coefficients $\alpha_L(E)$ defined in (24) for CuCu, which should ideally be equal to 1. They are without any singularity at the special energies (table 1) and their structures reflect those of $\bar{\Gamma}^{00}_{LL}(E)$ as can be seen for the symmetries d_{12} and $d_{25'}$, on figures 1 and 3. One can deduce from these curves that the discrepancy between the integrals $\bar{N}^0_L(E)$ and $N^0_L(E)$ is not constant through the valence band. Some compensation occurs above the 3d band, giving a good result at E_F. It is then obvious that for FeFe the numerical inaccuracy of (28) is more crucial, owing to the fact that the 3d bands for the two spins are not equally filled.

It must be noted that what we call here the intrinsic accuracy of the impurity program, i.e. its capacity to reproduce for the X 'impurity' the exact electronic structure of the X atoms of the matrix, is essentially limited by the numerical integration (28). This limitation is not specific to the LMTO theory but exists as well in the KKR formalism.

5.3. Examples

There are two ways to perform the self-consistent calculation for dilute alloys, either by constraining the defect to ensure the Friedel screening rule

$$Z - \bar{Z} = \sum_{\sigma} \left(N^{\sigma}_{C} - \bar{N}^{\sigma}_{C} + \frac{1}{\pi} \sum_{L} \Lambda^{\sigma}_{L}(E_F) \right) \tag{29}$$

(σ being the spin index), or without this constraint. In the first case the global neutrality of the crystal is ensured automatically, but this leads sometimes to too strong a local perturbation in the one-site approximation, where the impurity alone contributes to (29). In the second case the local perturbation may be weaker, but the crystal may not be neutral, which is also unphysical. This discrepancy vanishes when the first shells of neighbours of the impurity are included in the self-consistent calculation [14].

We give here some examples of the application of the LMTO method to dilute aluminium alloys, with and without the constraint (29). These calculations have been performed in the single-site approximation, the aim of this work being only to compare

our results (table 5(*a*)) to other calculations performed within the same hypothesis: those of Deutz *et al* [2] within the KKR formalism (table 5(*b*)) and those of Singh [8] by the LMTO method (table 5(*c*)).

Considering the small differences between our calculations and those of [2], such as (i) Von Barth–Hedin exchange–correlation potential instead of Moruzzi's one [15] and (ii) atomic sphere approximation instead of muffin-tin spheres, we can conclude that our LMTO results agree well with those of the KKR formalism in *any* case. The curious results obtained by Singh for the total displaced charge (i.e. for the values of $\Lambda_L(E_F)$) for Cu when enforcing the Friedel screening rule, and especially for Mn and Cr impurities, are certainly due neither to an intrinsic failure of the LMTO formalism nor to the single-site approximation.

6. Conclusion

We have in this paper analysed some aspects of the LMTO method applied to pure metals and dilute alloys. Our main conclusions are the following.

(i) The LMTO limit introduces singularities at special energies on functions that are regular in the KKR formalism. But this leads to no singularity in the calculated physical quantities, so that the results are always comparable to those of the KKR theory.

(ii) The differences between the matrix and the self-consistent impurity in the tests on fictitious alloys $\underline{X}X$ are not due to the lack of combined corrections in the impurity cell, but simply reflect the unavoidable difference in the numerical calculations of the number of electrons in the matrix and in the impurity cell. These tests give the order of magnitude of the intrinsic accuracy of these calculations.

(iii) Finally, we have presented evidence why the classical LMTO method with one panel for the conduction states is a very good method for the calculation of the electronic structure of pure metals, while the use of several panels and a Taylor series to third order for the wavefunction can be necessary for dilute alloys.

References

[1] Drittler B, Stefanou N, Blügel S, Zeller R and Dederichs P H 1989 *Phys. Rev.* B **40** 8203 and references therein
[2] Deutz J, Dederichs P H and Zeller R 1981 *J. Phys. F: Met. Phys.* **11** 1787
[3] Stefanou N, Oswald A, Zeller R and Dederichs P H 1987 *Phys. Rev.* B **35** 6911
[4] Koenig C and Daniel E 1981 *J. Physique* **42** L193
[5] Koenig C, Stefanou N and Koch J M 1986 *Phys. Rev.* B **33** 5307
Koch J M, Stefanou N and Koenig C 1986 *Phys. Rev.* B **33** 5319
[6] Koch J M and Koenig C 1988 *Phil. Mag.* B **57** 557
[7] Andersen O K 1975 *Phys. Rev.* B **12** 3060
Gunnarsson P, Jepsen O and Andersen O K 1983 *Phys. Rev.* B **27** 7144
[8] Singh P P 1991 *J. Phys.: Condens. Matter* **3** 3285
[9] Christensen N E and Kollar J 1983 *Solid State Commun.* **46** 737
Koenig C and Khan M A 1988 *Phys. Rev.* B **38** 5887
Knab D and Koenig C 1990 *J. Phys.: Condens. Matter* **2** 465
[10] Jepsen O and Andersen O K 1971 *Solid State Commun.* **9** 1763
[11] Harris R 1970 *J. Phys. C: Solid State Phys.* **3** 172
[12] Podloucky R, Zeller R and Dederichs P H 1980 *Phys. Rev.* B **22** 5777

[13] Koenig C 1973 *J. Phys. F: Met. Phys.* **3** 1497
Zeller R, Deutz J and Dederichs P H 1982 *Solid State Commun.* **44** 993
[14] Stefanou N, Oswald A, Zeller R and Dederichs P H 1987 *Phys. Rev.* B **35** 6911
[15] Moruzzi V L, Janak J F and Williams A R 1978 *Calculated Electronic Properties of Metals* (New York: Pergamon) pp 52–5
Von Barth U and Hedin L 1972 *J. Phys. C: Solid State Phys.* **5** 1629